ELSEVIER

Journal of Power Sources 112 (2002) 339–352

JOURNAL OF POWER SOURCES

www.elsevier.com/locate/jpowsour

Methanol crossover in direct methanol fuel cells: a link between power and energy density

Bogdan Gurau[a], Eugene S. Smotkin[b,*]

[a] *Department of Chemical and Environmental Engineering, Illinois Institute of Technology, 10 West 33 Rd Street, Chicago, IL 60616, USA*
[b] *Department of Chemistry, University of Puerto Rico at Rio Piedras, San Juan, Puerto Rico 00931, USA*

Received 9 July 2002; accepted 22 July 2002

Abstract

Direct methanol fuel cell performance curves were obtained as a function of three parameters, (1) temperature, (2) fuel flow-rate and (3) concentration. Methanol crossover was measured by gas chromatography as a function of these three parameters at 100 mA/cm^2 in the single-pass fuel delivery mode. The data was used to model a continuous loop mode where pure methanol is injected into a loop that circulates through the flow-field and recovers water from the cathode. The modeled loop composition is identical to the fuel stream used in the single-pass experiments (dilute aqueous methanol). The model results, presented in three-dimensional surfaces, elucidate the impact of parameter variations on the energy and power density of the direct methanol fuel cell (DMFC) and the link between those two figures of merit. In addition, a reasonable estimate of the contribution of mass transport effects due to the carbon fabric current collectors is made along with in situ CO stripping experiments on membrane electrode assembly (MEA) anode surfaces. The analysis shows that, at present, serious compromises are required if reasonable energy and power densities are to be simultaneously maintained in DMFCs using Nafion^{TM} 117 as an electrolyte.

Keywords: Direct methanol fuel cells; Gas chromatography; Parameter variations

1. Introduction

Liquid feed direct methanol fuel cells (DMFCs) are promising candidates for portable power applications. Methanol is a liquid at room temperature, has limited toxicity, is cheap and has a high energy density (3800 kcal/l) compared to hydrogen at 360 atm. (658 kcal/l). The DMFC does not require a fuel processor, permitting simple, compact designs [1,2]. Prototype DMFC stacks have been assembled [3–9] and intense efforts seek to identify optimum operating parameters (temperature, pressure, flow-rate, flow-field, catalyst loading, etc.) [10–14]. Methanol is oxidized at the anode concomitant with oxygen (i.e. air) reduction at the cathode:

$$CH_3OH + H_2O \rightarrow CO_2 + 6e^- + 6H^+ \quad \text{(anode)}$$

$$\tfrac{3}{2}O_2 + 6e^- + 6H^+ \rightarrow 3H_2O \quad \text{(cathode)}$$

$$CH_3OH + \tfrac{3}{2}O_2 \rightarrow CO_2 + 2H_2O \quad \text{(cell)}$$

Unlike hydrogen/air fuel cells, where essentially all of the polarization losses are at the cathode, DMFC polarization losses at the anode and cathode are comparable. Methanol oxidation kinetics are sluggish and renegade methanol crossing from the anode, through the polymer membrane, to the cathode catalytic layer further hampers oxygen reduction at the cathode. Methanol utilizes cathode Pt sites (reducing the effective area of the cathode) for the direct reaction between methanol and oxygen, which generates a mixed potential that reduces cell voltage [15,16], generates additional water that must be managed and increases the required oxygen stoichiometric ratio. In summary, methanol crossover severely impacts fuel utilization and must be mitigated.

The effect of crossover on fuel cell performance is intensely studied [17–20]. Los Alamos National Laboratories performed extensive MeOH permeation measurements through Nafion^{TM} 117 and 120 [21]. A strategy for mitigation of crossover is the development of new [22,15,23,24] or modification of existing membranes [25]. In spite of Herculean efforts to develop new polymers for DMFCs, Nafion^{TM} 117 is still the best polymer electrolyte for DMFCs. The inability to find better ionomers is linked to the operative mechanism for proton transport in the aqueous

* Corresponding author. Tel.: +1-787-764-0000x4796; fax: +1-787-764-1588.
E-mail address: esmotkin@goliath.cnnet.clu.edu (E.S. Smotkin).

0378-7753/02/$ – see front matter
PII: S0378-7753(02)00445-7

phase of ionomeric membranes (e.g. Nafion), namely, the Grotthuss mechanism, which involves very rapid hopping between neighboring sites involving $H_9O_4^+$ and $H_5O_2^+$ cluster ions [26]. The very low activation energies result from the high degree of cluster ion rotational freedom in bulk like water. As the Nafion water content is reduced, the Grotthuss mechanism becomes less operative and the transport mechanism for solvated protons approaches that of simple diffusion. The development of ionomers with low methanol diffusivities (methanol has a smaller stokes Einstein radius than the solvated proton) without compromising the rotational freedom of protonic clusters ions has proven to be very challenging.

Engineering approaches to the mitigation of methanol crossover must be complemented with materials development. Towards this end the effects of temperature (80, 60 and 40 °C),[1] aqueous methanol flow-rates (5, 0.5 and 0.15 ml/min) and MeOH concentrations (2, 1 and 0.5M) on methanol crossover has been investigated with a full fuel cell assembly (5 cm^2 electrodes). The cathode exhaust is analyzed by gas chromatography (GC) for carbonaceous species (derived from renegade MeOH). The complete mass balance characterization of steady state fuel cell operation is determined by GC and fuel cell current voltage (*i*–*V*) data over a wide variety of operating conditions. The data show that judicious selection of fuel cell operating parameters must be complemented with membrane electrode assembly (MEA) and flow-field design improvements if methanol crossover is to be mitigated using state-of-art polymer electrolyte membranes.

2. Experimental

The single cell DMFC system is schematized (Fig. 1). The graphite blocks (POCO Graphite Inc., Decatur, Texas) have triple channel serpentine flow-fields at both the anode and cathode sides. A high precision computerized syringe pump (Isco Inc., Lincoln, NE) meters aqueous MeOH to the anode flow-fields, while a mass flow controller (MKS Instruments, Andover, MA) meters dry air to the cathode flow-field (20.0 ml/(min cm^2) at ambient pressure).

The cathode exhaust components are monitored by a Perkin-Elmer Auto-System GC (Shelton, CT) equipped with automated gas sampling valves (Valco Instruments Co. Inc, Houston, TX). A thermal conductivity detector is used in series with a flame ionization detector.

The membrane electrode assembly (MEA) consists of a polymer electrolyte membrane (Nafion™ 117 DuPont, South Duart, NC) sandwiched between anode and cathode catalytic layers. Electrical contacts between the two catalytic layers and the graphite flow-field blocks are maintained by the use of porous carbon diffusion layers (E-TEK Inc., Natick, MA). Toray paper (TGPH 060) is used on the anode side and ELAT 20% wet-proofed carbon cloth on the cathode side. The carbon paper and cloth, designed to maintain electrical contact while not impeding mass transport of electrode reactants and products from the flow-fields and electrode surfaces, are referred to as the gas diffusion layers (GDL). In fact, GDLs, designed for hydrogen air fuel cells, were not designed for liquid feed systems. Unsupported PtRu (BET surface area 83 m^2/g) and Pt-black (Alfa-Aesar, Ward Hill, MA) are used at the anode and cathode, respectively. Catalyst inks were prepared by mixing appropriate amounts of the black catalysts, Nanopure™ water (18.3 MΩ cm) and 5% Nafion™ solution (Aldrich, Milwaukee, WI).

The GDL catalyst loading was 4 mg/cm^2. The anode and cathode catalyzed GDLs were hot-pressed onto opposite faces of Nafion™ 117 (DuPont, South Duart, NC), resulting in a GDL integrated MEA (Fig. 1). Heating rods (Watlow, St. Louis, MO) and T-type thermocouples mounted into the graphite blocks control the cell temperature. Metallic end plates (not shown in Fig. 1) serve as electrical contacts and maintain uniform compression of the fuel cell assembly upon application of the desired torque at the connecting tie-rod bolts. Fuel cell performance data acquisition begins after 2 days of cell conditioning [27] at high current densities. Steady state polarization curves were obtained galvanostatically with a computer controlled load unit (Series 890B, Scribner Associates Inc., Southern Pines, NC). Data points were recorded only after steady state was obtained (ca. 4–5 min per point). Anode polarization data was obtained by operating the fuel cell galvanostatically (a 5 V dc power supply was placed in series with the cathode) with humidified H_2 delivered to the cathode, which doubled as a dynamic hydrogen reference electrode.

In situ fuel cell CO stripping measurements quantified the electrochemically active surface area. The anode was set at 0.1 V and CO (1% balanced Ar) was passed through the anode chamber for 30 min followed with pure N_2 for another 30 min. The CO stripping wave, and background, was obtained by sweeping from 0.1 to 0.0 V followed by 2 cycles from 0 to 1.2 V. At all times H_2 was passed through the cathode and the cell was maintained at 60 °C. Cyclic voltammograms were obtained using an Autolab potentiostat (Brinkmann Instruments, NY). Five stripping experiments were analyzed to ensure reproducibility.

3. Results and discussion

Figs. 2–4 show DMFC performance at 80, 60 and 40 °C, respectively, with the full fuel cell performance curves (lower panels) as well as the anode and cathode polarization curves split out (upper panels). At each temperature, three

[1] From a practical perspective there are a wide range of devices that span such a broad range of operational conditions. For example, the small power devices (cell phones, PDAs, etc.) will operate at 40 °C or lower, while intermediate power devices (notebook computers, power tools, battery chargers for army or remote site applications) will more likely operate at higher temperatures (60–80 °C).

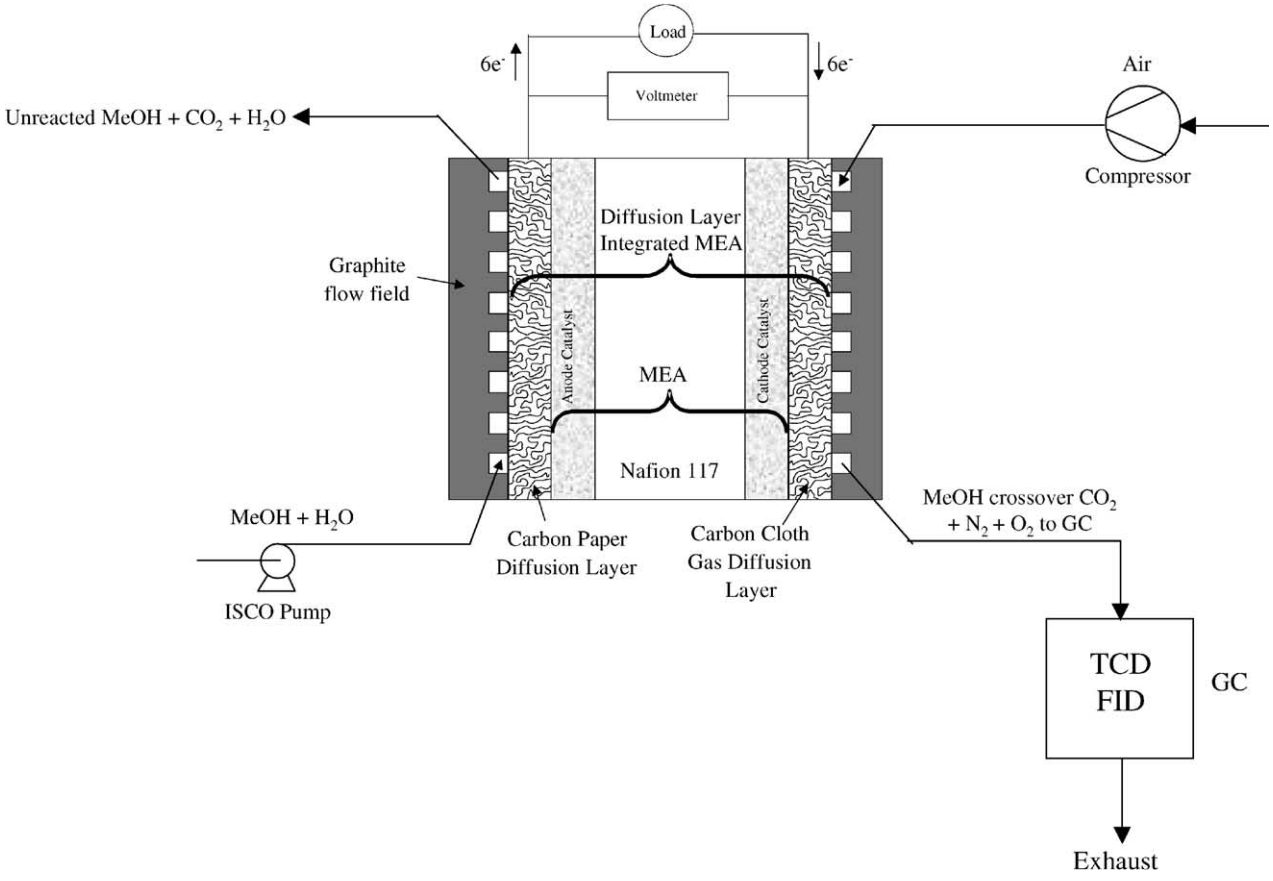

Fig. 1. Experimental set-up for the DMFC experiments.

flow-rates are studied at three methanol concentrations. Thus, 27 operating conditions are represented in Figs. 2–4.

The fuel cell temperature was varied with 0.5 M methanol at 1 ml/min for determination of the anode process activation energy in a genuine fuel cell environment. The PtRu anode has an Arrhenius temperature dependence (Fig. 5 upper line) with an activation energy of 30 kJ/mol. This differs from the 60 kJ/mol value reported by Wieckowski studying Ru ''decorated'' single crystal Pt in aqueous acid [28]. Several factors may be involved. Methanol oxidation kinetics on Nafion-coated electrodes, immersed in acidic aqueous electrolytes is enhanced relative to uncoated electrodes [29]. Fuel cell MEA catalyst particles are encased in Nafion, which provides a superacidic environment absent of mobile anions that can contribute to anion poisoning. No FTIR evidence that the Nafion backbone-anchored sulfonate groups adsorb to (and thus poison) the Pt surface was observed [30]. Specular reflectance data show lower Stark tuning rates for CO adsorbed on high surface area PtRu than on polished arc-melted PtRu alloys [31,32]. Although we cannot yet relate the Stark tuning data to the activation energy discrepancy, there may be significant differences between the electronic interactions of adsorbed intermediates with smooth electrodes in aqueous acidic environments versus with nanostructured catalysts encased in Nafion with no mobile anions.

The full fuel cell performance data does appear to have Arrhenius behavior (Fig. 5 lower curve) because the cathode performance is attenuated by methanol crossover and much of the gains at the cathode, expected with increasing temperature, are lost because the membrane permeability increases with temperature. The Arrhenius plot flattens as the temperature is increased and this is consistent with a direct relationship between methanol permeability and temperature.

At low current densities, the cell voltage decreases as the flow-rate increases. This is most evident at open circuit where the sensitivity of the cell voltage to the flow-rate is maximal. This confirms a direct relationship between flow-rate and crossover. However, over the range of flow-rates studied, changes in the pressure drop through the flow-field could not be detected using a pressure gage with a range of 0–3.5 psi. This suggests that the activity of methanol at the catalyst layer (even at open circuit where all the consumption is due to crossover) is very sensitive to flow-rate. As the current density is increased, methanol crossover decreases since oxidation of methanol at the anode diminishes the activity of methanol at the anode surface and thus reduces

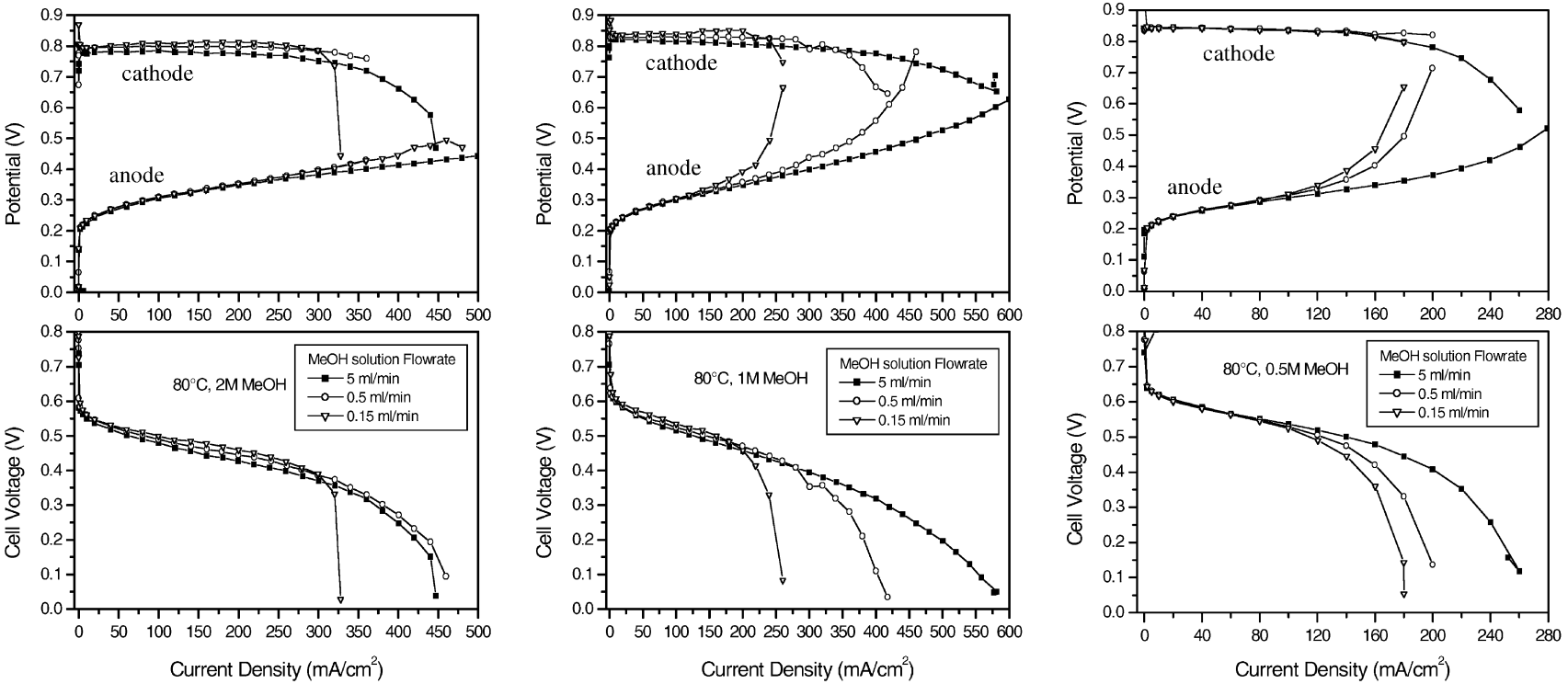

Fig. 2. DMFC performance at 80 °C at various MeOH concentrations and fuel flow-rates.

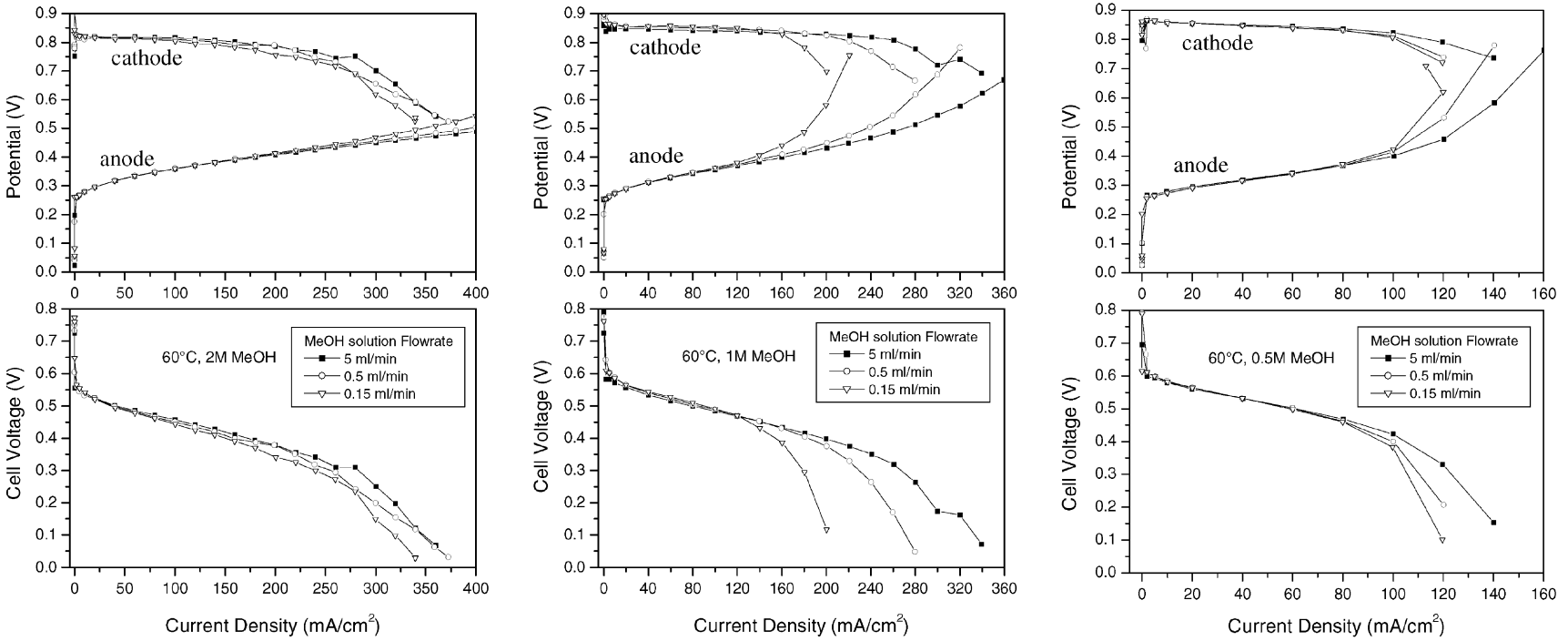

Fig. 3. DMFC performance at 60 °C at various MeOH concentrations and fuel flow-rates.

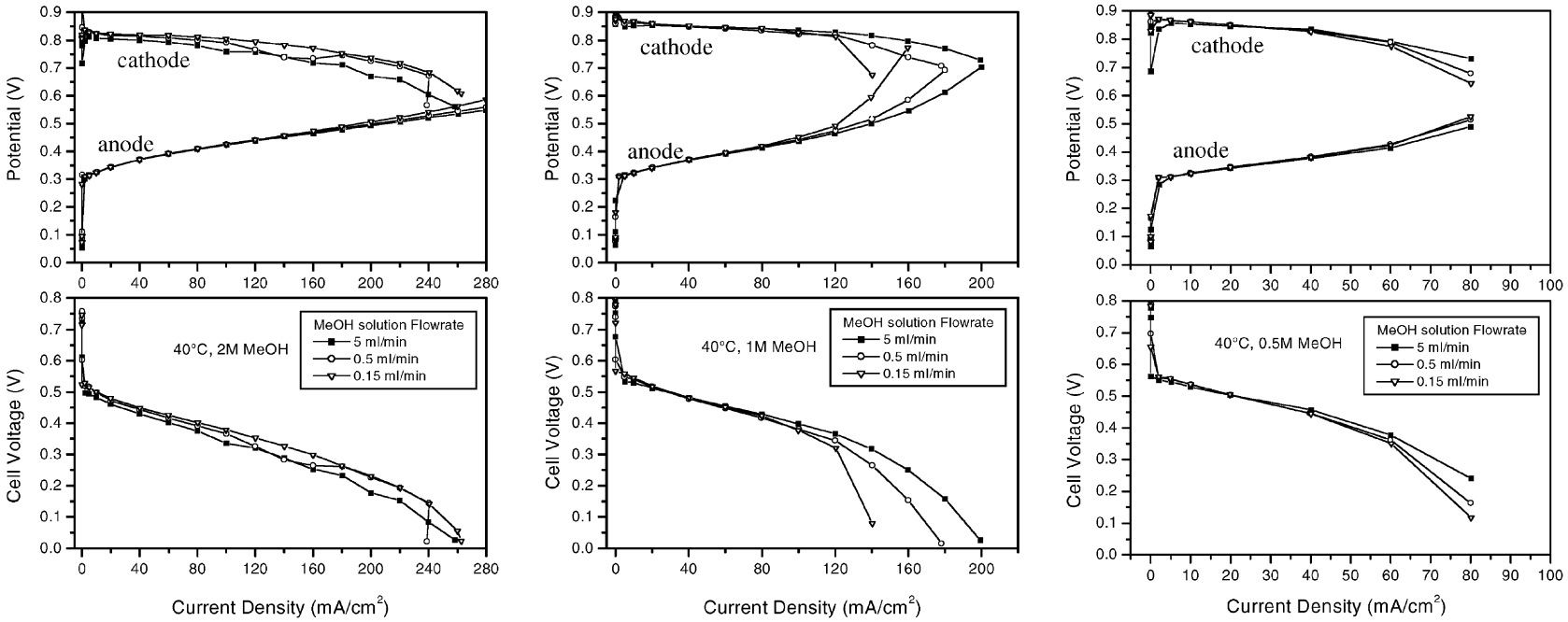

Fig. 4. DMFC performance at 40 °C at various MeOH concentrations and fuel flow-rates.

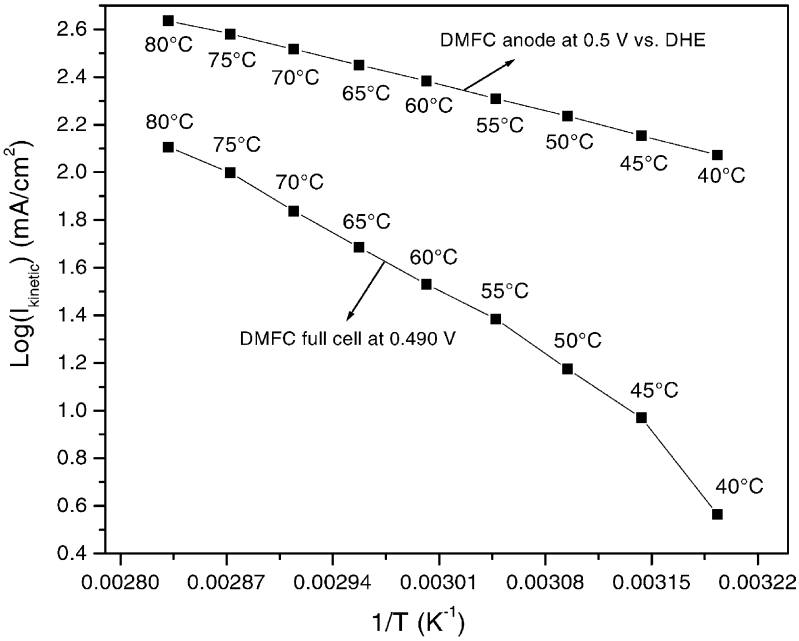

Fig. 5. Anode and full fuel cell performance as a function of temperature at constant potentials (arbitrary chosen).

the Ficks' law gradient of methanol across the membrane [33,34].

Carbon cycle data for a DMFC can be represented in two ways (1) ''single-pass'' and (2) ''continuous loop''. The single-pass mode is often used in laboratory studies where fuel is passed through the anode flow-fields and then directly to waste. Analysis of single-pass data permits the modeling of the continuous loop mode, which is the mode to be used in

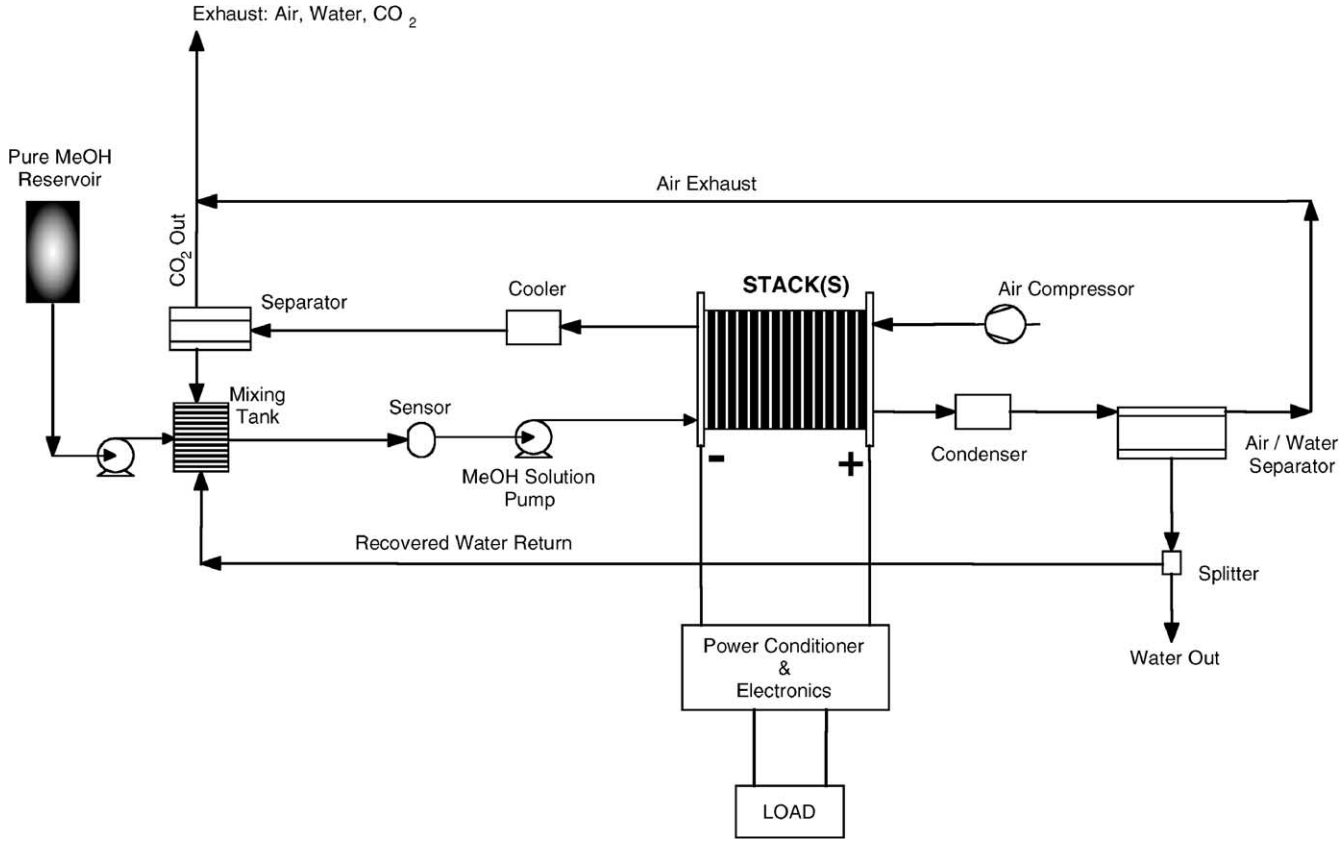

Fig. 6. DMFC system schematic showing continuous loop mode.

commercialized systems. Single-pass conversions are calculated as follows:

$$X_{\mathrm{F}} = \frac{V_{\mathrm{F}}}{V_{\mathrm{inlet}}} \times 100$$

$$X_{\mathrm{xo}} = \frac{V_{\mathrm{xo}}}{V_{\mathrm{inlet}}} \times 100$$

$$X_{\mathrm{Ex}} = 100 - X_{\mathrm{F}} - X_{\mathrm{xo}}$$

where X_{F} is the fraction of MeOH Faradaically oxidized at the anode, X_{xo} the fraction of MeOH oxidized as renegade methanol at the cathode, X_{Ex} the fraction of MeOH exiting the anode to waste, V_{F} the volumetric flow-rate of the MeOH converted Faradaically in the anode reaction, V_{xo} the volumetric flow-rate of the crossover MeOH and V_{inlet} is the fuel cell inlet volumetric flow-rate of MeOH.

The continuous loop method involves blending of the anode exhaust stream with pure methanol to replace the methanol lost to crossover and the methanol consumed Faradaically. In addition water is returned from the cathode side to replenish water used in the anode reaction and water lost to electroosmotic drag. The replenished fuel is fed back to the fuel cell inlet. In this mode there are only two modes of methanol consumption, Faradaic oxidation and methanol crossover. Fig. 6 schematizes a DMFC system incorporating a continuous loop with fuel injection of pure methanol. The loop includes the mixing tank, sensor, fuel pump, anode flow-field, cooler, separator and mixing tank. Pure methanol is injected into the loop to replenish methanol oxidized at the anode and lost to crossover. The global Faradaic MeOH conversion and the fraction of MeOH lost to crossover in the continuous loop mode are calculated using the following formulas:

$$X_{\mathrm{GF}} = \frac{V_{\mathrm{F}}}{V_{\mathrm{F}} + V_{\mathrm{xo}}}$$

$$X_{\mathrm{GXO}} = 100 - X_{\mathrm{GF}}$$

where X_{GF} is the global Faradaic conversion of MeOH, X_{GXO} the fraction of MeOH lost to crossover and V_{F} and V_{xo} have the same meaning as above. The global conversion represents the final conversion and the fuel efficiency for the continuous loop mode.

Data from Figs. 2–4, at 100 mA/cm^2, was used to calculate and illustrate the carbon cycle dependence on the methanol concentration and flow-rate at 80, 60 and 40 °C (Figs. 7–9, respectively). At each concentration, the top triad of pie charts show the carbon balance experimentally

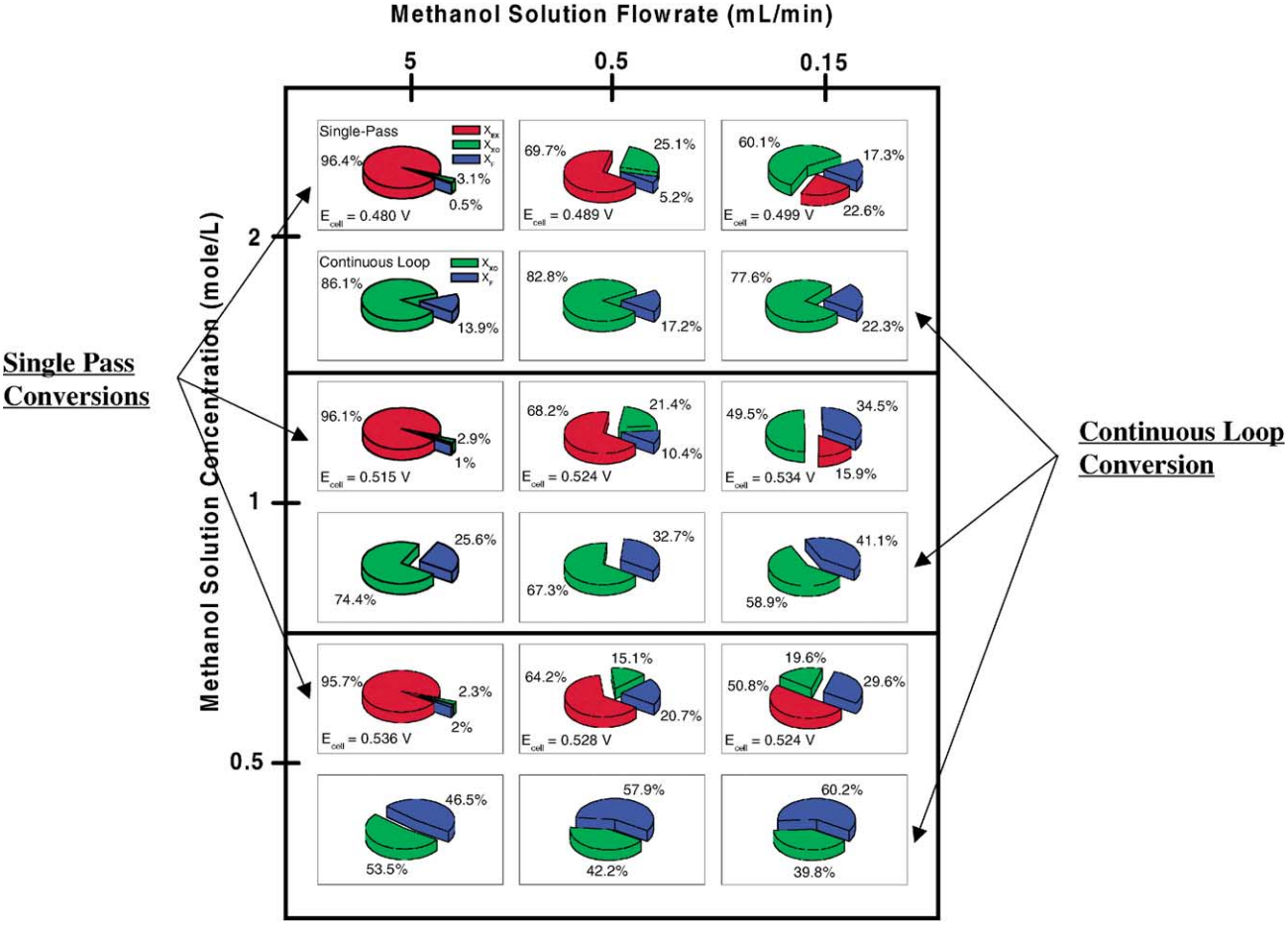

Fig. 7. Flow-rate and concentration dependence of MeOH conversion at 80 °C, 100 mA/cm^2.

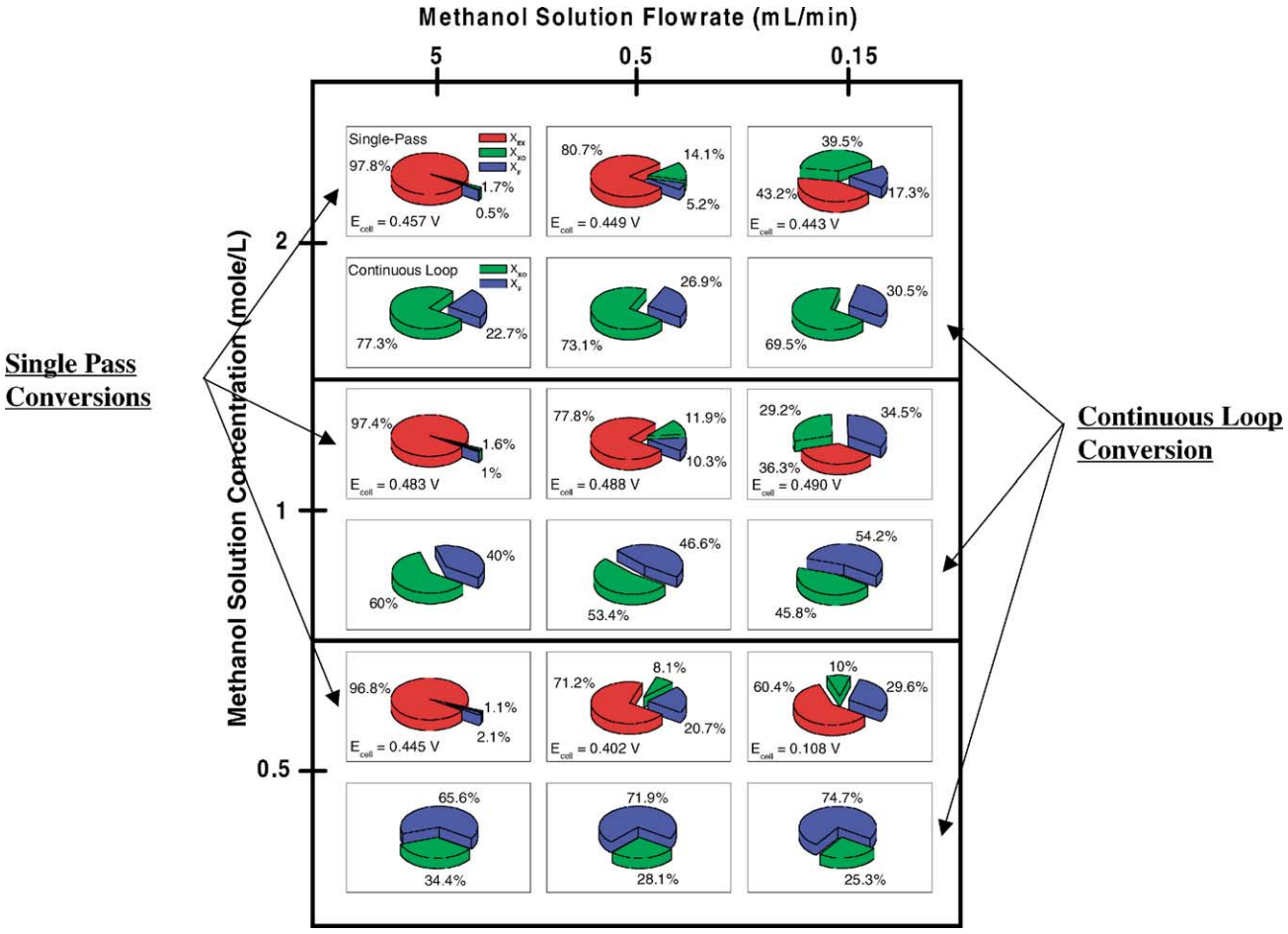

Fig. 8. Flow-rate and concentration dependence of MeOH conversion at 60 °C at 100 mA/cm^2.

determined using the fuel cell test stand interfaced to a gas chromatograph. The top three pie segments include exhaust methanol waste, crossover methanol and Faradaically oxidized methanol. The lower triad of pie charts show the calculated continuous loop conversions calculated from the single-pass data. The lower triad pie charts have only two segments because no methanol exhausts to waste in the continuous loop mode.

Figs. 7–9 show a strong dependence of continuous loop fuel efficiency upon the cell temperature and fuel flow-rate. The methanol loss due to crossover are reduced from 86% @ 2M, 0.5 ml/min to 40% @ 0.5M, 0.15 ml/min at 80 °C. The losses diminish further as the temperature is reduced (i.e. permeability of methanol is decreased). At 40 °C the crossover loss is only 17% at 0.5M, 0.15 ml/min.

Fuel efficiency is not the only criterion for performance optimization. The device power requirements must be met by the fuel cell. The continuous loop Faradaic fuel conversion *and* the cell voltage must be considered simultaneously versus four independent DMFC operational parameters: (1) MeOH concentration, (2) fuel flow-rate, (3) current density and (4) temperature. The optimum temperature and current density are application dependent. The display of data surfaces was limited to three dimensions by selection of three temperatures (i.e. three sets of surfaces) at a current density of 100 mA/cm^2 to illustrate all of the parameter dependent crossover issues (Figs. 10–12).

At 80 °C (Fig. 10) the power density is greatest at the lowest MeOH concentration and the highest flow-rate (i.e. 0.5 M and 5 ml/min). However, at this operating point the energy density is low (47%) due to fuel crossover. The lowering of the flow-rate from 5 to 0.15 ml/min results in a cell voltage loss of only 9 mV, which has negligible effect on the DMFC stack size while substantially improving the MeOH conversion (ca. 47–58%), increasing the energy density and reducing parasitic losses due to the fuel re-circulation pump. Overall, at 80 °C the fuel conversion is unacceptably low due to crossover. Unless better membranes are developed, liquid feed DMFCs at 80 °C cannot be commercialized.

The fuel conversion surfaces improve substantially with decreasing temperature. Although the landscape of the fuel conversion surfaces does not change significantly with temperature, the entire surface elevates to higher conversions as the temperature is reduced. In sharp contrast, the cell voltage landscape dramatically changes with decreasing temperature: *the landscape inverts*. Thus, at 80 °C the high voltage regime overlaps with the high fuel conversion regime (Fig. 10) while at the lower temperatures (Figs. 11 and 12)

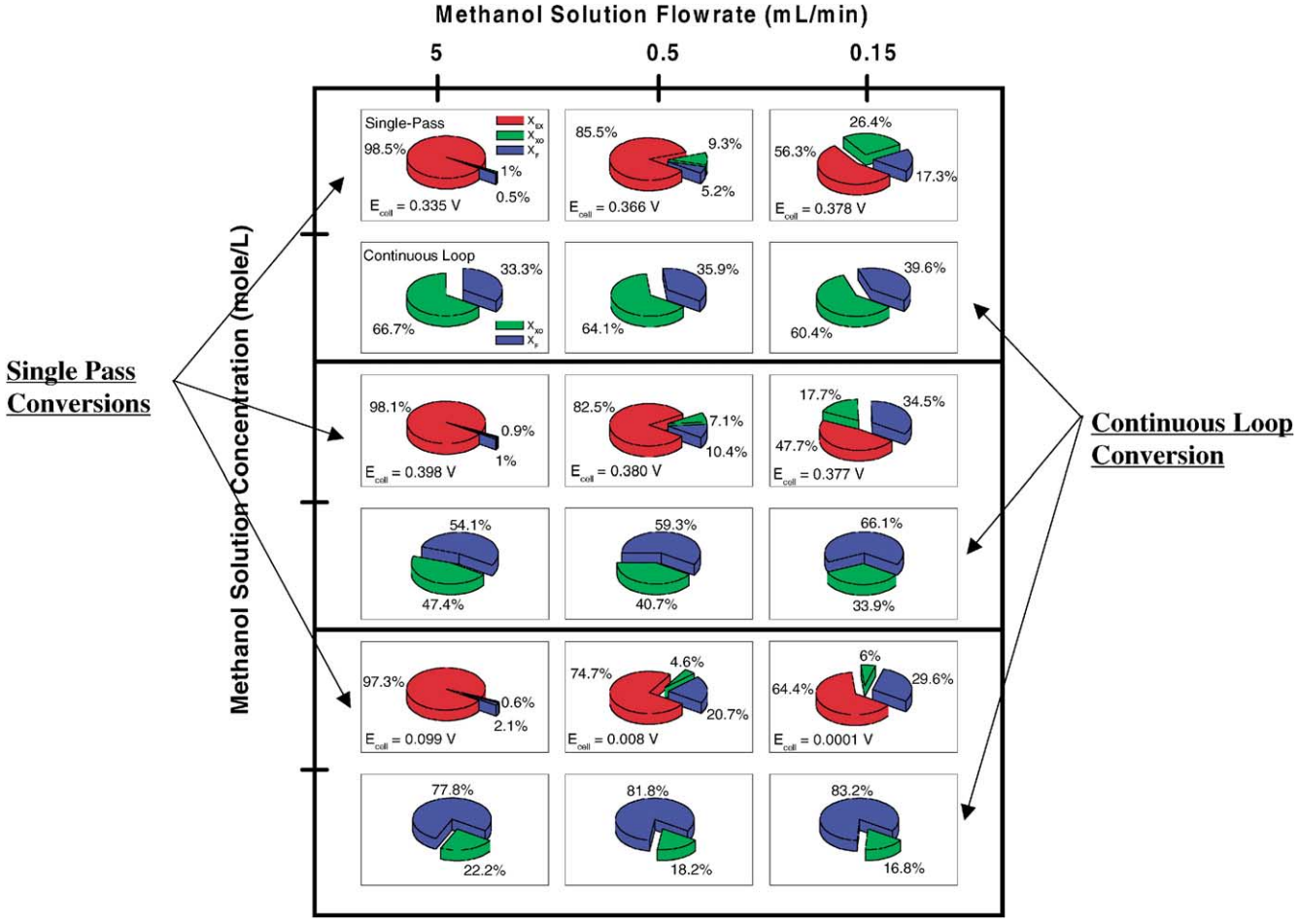

Fig. 9. Flow-rate and concentration dependence of MeOH conversion at 40 °C at 100 mA/cm^2.

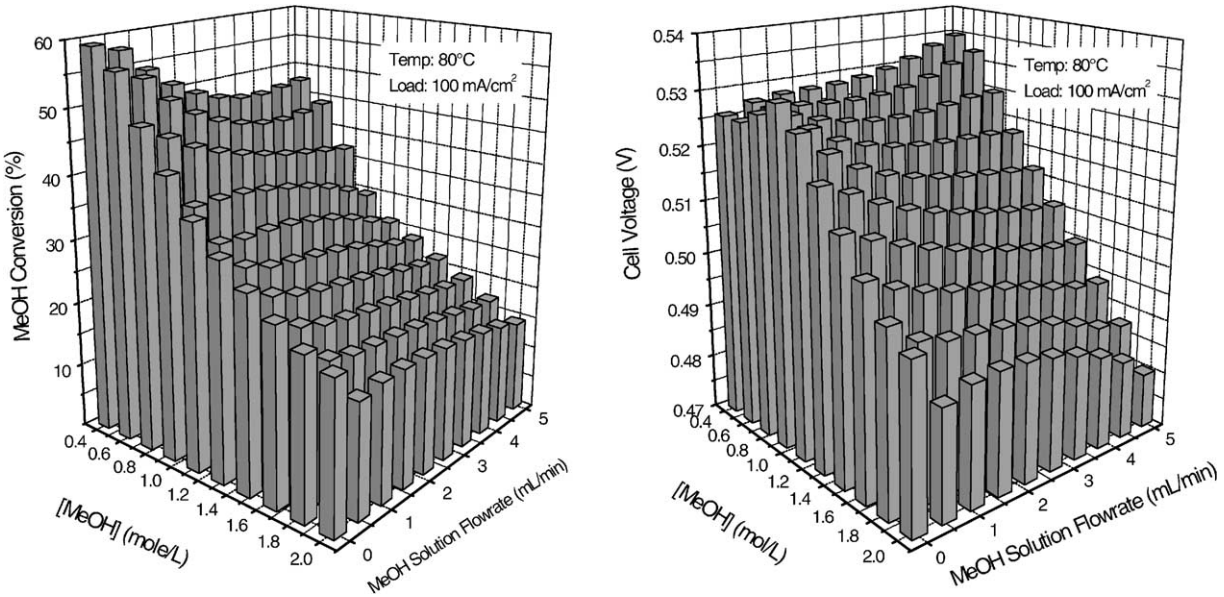

Fig. 10. 3D DMFC performance at 80 °C at various MeOH concentrations and fuel flow-rates under constant load.

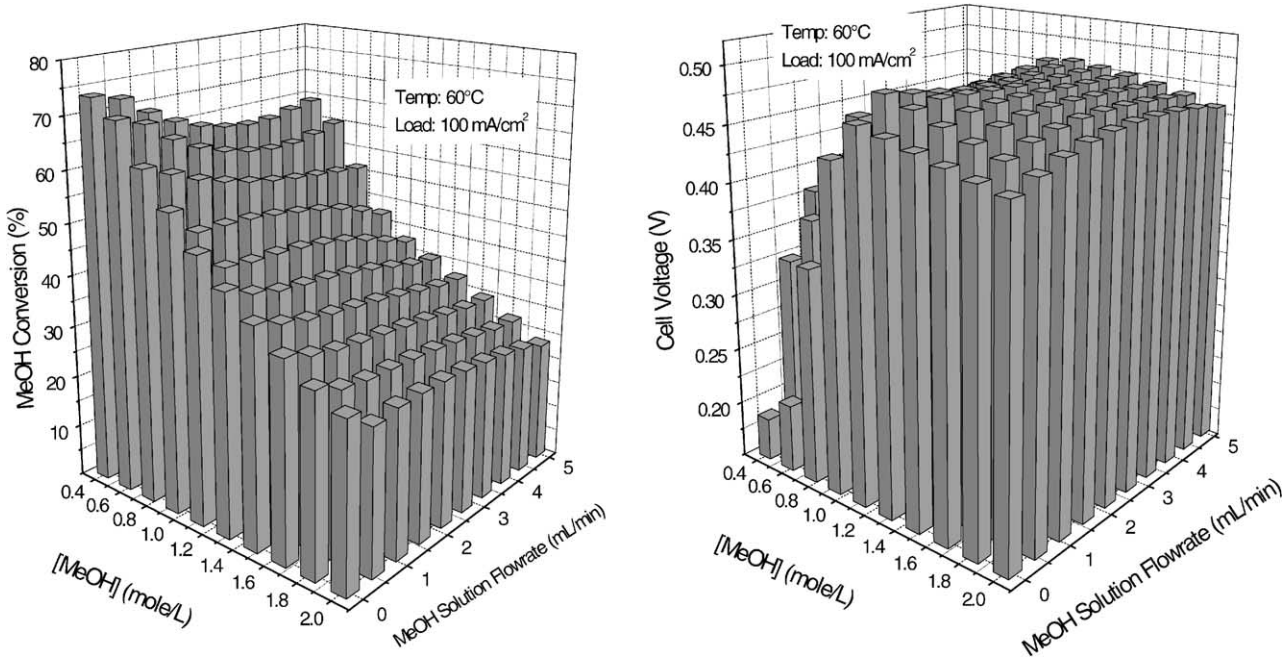

Fig. 11. 3D DMFC performance at 60 °C at various MeOH concentrations and fuel flow-rates under constant load.

the cell voltages are lowest where the fuel conversion rates are highest. At 60 and 40 °C, the cell voltages at maximum fuel utilization (73 and 82%, respectively) are 0.1 and 0.02 V (essentially at short circuit). Thus, with state-of-art membranes, fuel utilization (i.e. energy density) must be substantially sacrificed for the sake of power density (Table 1). This is evident when selecting operating conditions on the basis of power density. At 60 °C the maximum power density is at 1.1 M and 0.5 ml/min flow-rate but the MeOH conversion is 45%. At 40 °C the maximum power density is at approximately 1.3 M with a flow-rate of 5 ml/min with 50% of the methanol lost to crossover. Table 1 shows the maximum power point (as cell voltage at 100 mA/cm^2) and the corresponding methanol conversion. Table 2 shows the maximum methanol conversion and the corresponding cell voltage at 100 mA/cm^2.

This data shows that a substantial compromise in energy density is required if high power density systems are to be

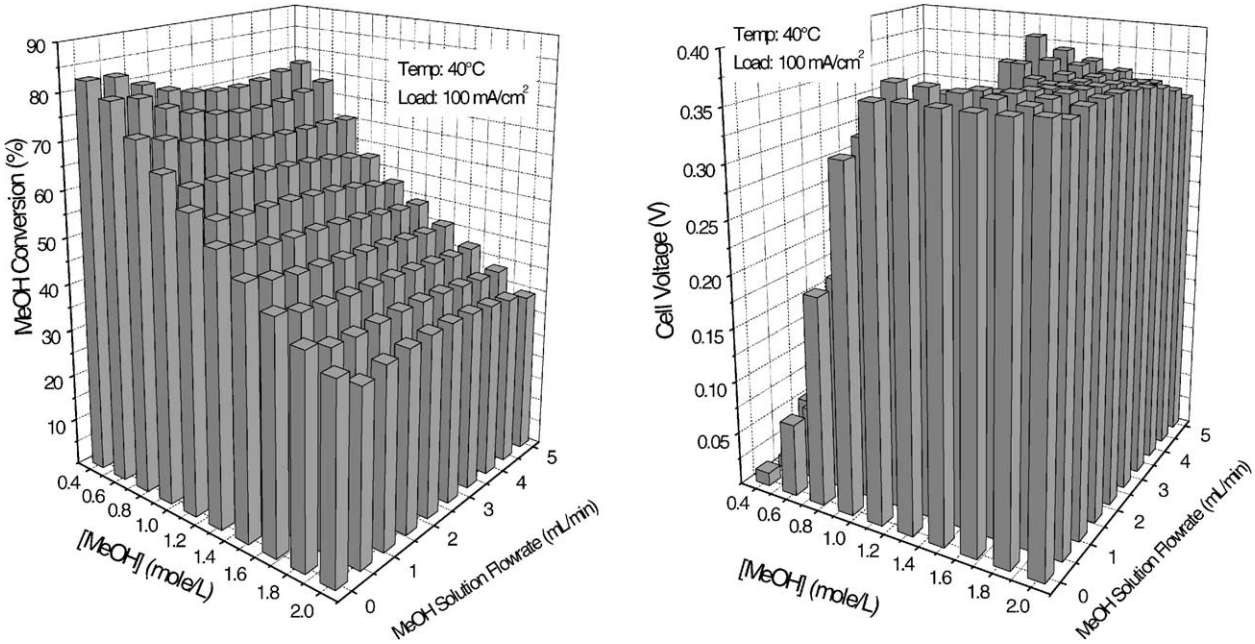

Fig. 12. 3D DMFC performance at 40 °C at various MeOH concentrations and fuel flow-rates under constant load.

Table 1
Power density maximum (at 100 mA/cm^2)

	Temperature (°C)		
	80	60	40
Cell voltage (V)	0.534	0.455	0.380
Methanol conversion (%)	47	45	50

Table 2
Energy density maximum (at 100 mA/cm^2)

	Temperature (°C)		
	80	60	40
Methanol conversion (%)	58	73	82
Cell voltage (V)	0.525	0.120	0.020

designed with Nafion™ 117. It is important to note that the selection of 100 mA/cm^2 for the above analysis was arbitrary. Coupled with GC data, the data of Figs. 2–4 can be used for the above analysis at any current density. Analysis of the above data would benefit from the selection of a more general "figure of merit" variable coupled with data mining software capable of incorporating all of the operational variables simultaneously.

The single-pass conversion data illustrates another DMFC engineering obstacle: the electrodes are heavily mass transport affected. Consider the anode polarization curve for 1 M MeOH, 0.5 ml/min, 80 °C (Fig. 2). Fig. 13 shows the mass transport corrected data. The stoichiometric ratio (SR) is defined as:

$$\mathrm{SR} = \frac{F_{\mathrm{inlet}} C_{\mathrm{inlet}}}{i A_{\mathrm{el}}/6F}$$

where F_{inlet} is the volumetric flow-rate of MeOH at the inlet of the anode chamber, C_{inlet} the MeOH inlet feed concentration, i the current density, A_{el} the geometric area of the electrode and F is Faraday's constant. The mass transport correction is applied using the well-known formula [35]:

$$i_{\mathrm{kin}} = \frac{i_{\mathrm{a}} i_{\mathrm{lim}}}{i_{\mathrm{lim}} - i_{\mathrm{a}}}$$

where i_{kin} is the kinetic current density, i_{a} the observed anodic current and i_{lim} is the methanol oxidation limiting current. The experimental polarization curve is mass transport affected as early as 50 mA/cm^2. At the selected operating point (100 mA/cm^2) there is an increase in over-potential of about 10 mV due to mass transport effects in spite of a stoichiometric ratio of >10.

CO stripping experiments were performed to determine the electrocatalytically active area corresponding to the geometric area of the MEA electrode. Fig. 14 shows two successive scans: the first scan removes the adsorbed CO on the surface and the second scan is used as baseline for integration of the CO stripping peak. The electrochemically active area of the MEA electrode (A_{act}) is calculated as follows:

$$A_{\mathrm{act}} = \frac{Q_{\mathrm{meas}}}{Q_{\mathrm{mono}}}$$

The integral of the stripping wave (volts × amps) divided by the scan rate (0.005 V/s) is Q_{meas} and has dimensions of coulombs. The charge required to oxidize a monolayer of linearly adsorbed CO on Pt is Q_{mono} (≈4 C/m^2) [36]. The mean value of the calculated A_{act} is 0.84 m^2. At this time we cannot apportion out the fraction of CO oxidized on the surface area of the Ru component of the mixed metal catalysts. Our FTIR data from previous work does show

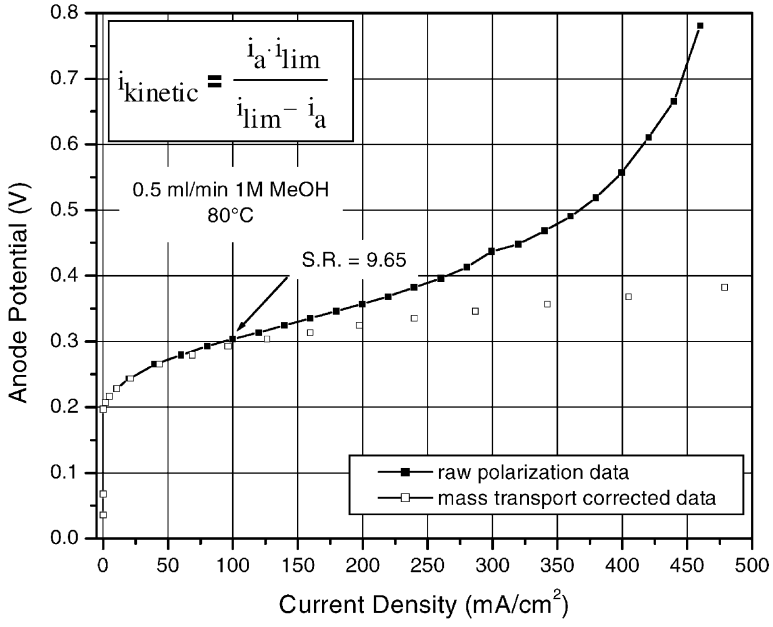

Fig. 13. Mass transport correction of the anode polarization data.

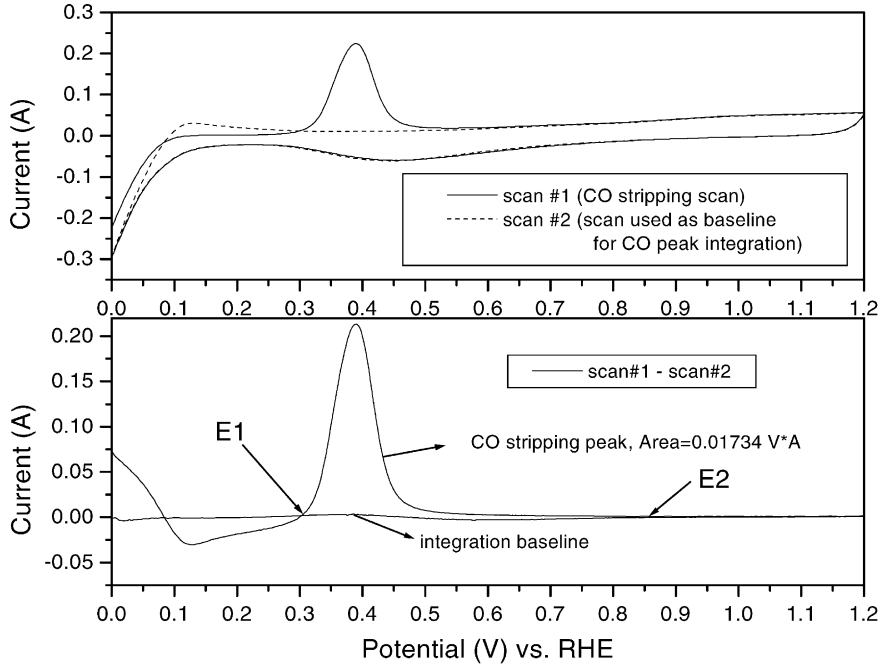

Fig. 14. Cyclic voltammogram for the CO stripping experiment. E1 and E2 in the lower panel represent the integration limits for the stripping scan.

that the coverage on Ru is substantially lower than on Pt [37].

The BET surface area of the unsupported PtRu particles (Johnson Matthey reports 80.6 m^2/gm) and the typical catalyst loading in a 5 cm^2 MEA anode (0.013 g) determines the MEA BET surface area (A_{BET}), which is typically 1.0 m^2. We define the fraction of the BET surface area that is electrochemically active for CO oxidation as A_{act}/A_{BET}. This fraction is about 80%. This is a very high utilization rate considering that the catalyst is 50 mol% Ru. This is consistent with the observation of CO adsorption and oxidation on MEA anodes catalyzed with Ru black [38].

A smooth electrode of roughness factor 1 having an area of 0.84 m^2 would yield a limiting current of over 1000 A. The measured value of 2.4 A is lower because the electrode is a porous electrode with a geometric area of 5 cm^2. In addition to the concentration gradient across the depth of the porous electrode, the carbon paper GDL also imposes mass transport limitations. Assuming an active area equal to the geometric area (5 cm^2) and no GDL mass transport effects, the following equation can be used:

$$i_{lim} = nFA_{geom}m_0c_{bulk}$$

The bulk concentration of MeOH (c_{bulk}) is 10^3 mol/m^3, n is the number of electrons exchanged in the anodic reaction (i.e. 6), F the Faraday's constant (96498 C/eq.), m_0 the mass transfer coefficient (i.e. D_{MeOH}/δ (m/s)), D_{MeOH} the diffusion coefficient of MeOH in water (2.8×10^{-9} m^2/s), δ is the thickness of the diffusion material (1.27×10^{-4} m). The calculated value for i_{lim} is 6.4 A. Thus, the limiting current is reduced by about a factor of 2–3 as a result of the GDL. The ramifications of this impedance can be illustrated by examination of Fig. 13. The rule of thumb is that currents at 10% or less of the limiting current are essentially kinetic. At 50 mA/cm^2, where the current is about 10% of the limiting current, the experimental data begins to diverge from the mass transport corrected data. If losses due to the GDL were removed (increasing the limiting current by a factor of about 3), the currents would be kinetic up to about 150 mA. Fig. 13 shows a loss of about 25 mV at 150 mA as a result of GDL mass transport effects. Although this is significant, catalysis remains the primary obstacle to DMFC commercialization when Nafion^{TM} 117 is used. When low crossover membranes are developed, improved performance at the cathode will permit polarization of the anode to more positive potentials. This will increase the contribution of C–H activation (as water activation improves with increased potential) to the rate-limiting step, changing the catalysis issues substantially [39].

4. Conclusions

DMFC performance is strongly dependent on a variety of factors including the membrane electrode assembly temperature, MeOH solution concentration and flow-rate. MeOH crossover, the rate of which depends on the above parameters, adversely affects fuel efficiency by wasteful oxidation at the cathode side while seriously depolarizing the cathode. Low fuel flow-rates and low concentrations enable very high fuel efficiencies (i.e. energy densities). However, mass transport limitations prevent the attainment of useful power densities under those conditions that enable high fuel efficiencies.

The electrochemically active area of the PtRu catalyst is determined from CO stripping experiments and the catalyst utilization is estimated to be very high (80%). The carbon paper GDL introduces a mass transport barrier that reduces fuel cell limiting currents by a factor of 2–3.

Acknowledgements

Thanks are due to Dr. Antonino Arico at CNR-ITAE, Messina, Italy and Dr. S.R. Narayanan at JPL for helpful comments. The Collaborative Technology Alliance Program of the Army Research Laboratories and NuVant Systems provided funding for this project.

References

[1] A. Hamnett, Philos. Trans. R. Soc. Lond., Ser. A 354 (1996) 1653.
[2] A.K. Shukla, P.A. Christensen, A.J. Dickinson, A. Hamnett, J. Power Sources 76 (1998) 54.
[3] P. Argyropoulos, K. Scott, W.M. Taama, J. Power Sources 79 (1999) 169.
[4] M. Baldauf, W. Preidel, J. Power Sources 84 (1999) 165.
[5] A.K. Shukla, M.K. Ravikumar, M. Neergat, K.S. Gandhi, J. Appl. Electrochem. 29 (1999) 131–132.
[6] D. Buttin, M. Dupont, M. Straumann, R. Gille, J.-C. Dubois, R. Ornelas, G.P. Fleba, E. Ramunni, V. Antonucci, A.S. Arico, P. Creti, E. Modica, M. Pham-Thi, J.-P. Ganne, J. Appl. Electrochem. 31 (2001) 278.
[7] X. Ren, P. Zelenay, S. Thomas, J. Davey, S. Gottesfeld, J. Power Sources 86 (2000) 113.
[8] P. Argyropoulos, K. Scott, W.M. Taama, J. Power Sources 87 (2000) 155.
[9] S.V. Andrian, J. Meusinger, J. Power Sources 91 (2000) 196–200.
[10] K. Scott, W.M. Taama, P. Argyropoulos, J. Power Sources 79 (1999) 51.
[11] A.S. Arico, P. Creti, P.L. Antonucci, J. Cho, H. Kim, V. Antonucci, Electrochim. Acta 43 (24) (1998) 3727.
[12] A.S. Arico, P. Creti, V. Baglio, E. Modica, V. Antonucci, J. Power Sources 91 (2000) 205.
[13] C.K. Witham, W. Chun, T.I. Valdez, S.R. Narayanan, Electrochem. Solid State Lett. 3 (11) (2000) 500.
[14] A.S. Arico, A.K. Shukla, K.M. El-Khatib, P. Creti, V. Antonucci, J. Appl. Electrochem. 29 (1999) 672–676.
[15] J.-T. Wang, S. Wasmus, R.F. Savinell, J. Electrochem. Soc. 143 (4) (1996) 1239.
[16] K. Kordesch, G. Simader, Fuel Cells and Their Applications, VCH, Weinheim, 1996.
[17] A. Heinzel, V.M. Barragan, J. Power Sources 84 (1999) 71–73.
[18] J. Cruickshank, K. Scott, J. Power Sources 70 (1998) 42–46.
[19] T.I. Valdez, S.R. Narayanan, Electrochem. Soc. Proc. 98 (27) (1998) 382–384.
[20] A. Kuver, W. Vielstich, J. Power Sources 74 (1998) 216–217.
[21] X. Ren, T.E. Springer, T.A. Zawodzinski, S. Gottesfeld, J. Electrochem Soc. 147 (2) (2000) 469–472.
[22] M. Walker, K.-M. Baumgartner, M. Kaiser, J. Kerres, A. Ulrich, E. Rauchle, J. Appl. Polym. Sci. 74 (1999) 70–71.
[23] H. Uchida, Y. Mizuno, M. Watanabe, Chem. Lett. (2000) 1268–1269.
[24] G.A. Deluga, S.C. Kelley, B. Pivovar, D.A. Shores, W.H. Smyrl, in: IEEE Proceedings of the fifteenth Annual Battery Conference on Applications and Advances, 1999 (2000) 51–53.
[25] W.C. Choi, J.D. Kim, S.I. Woo, J. Power Sources 96 (2001) 412–414.
[26] Peter Atkins, Physical Chemistry, 6th ed., Freeman, New York, 1999, p. 741.
[27] R. Viswanathan, G. Hou, R. Liu, S.R. Bare, F. Modica, G. Mickelson, C.U. Segre, N. Leyarovska, E.S. Smotkin, J. Phys. Chem. B 106 (13) (2002) 3458–3465.
[28] B. Grzybowska, P. Kulesza, G. Tremiliosi-Filho, H. Kim, W. Chrzanowski, A. Wieckowski, J. Electroanal. Chem. 143 (1999) 467.
[29] L. Liu, R. Viswanathan, R. Liu, E.S. Smotkin, Electrochem. Solid State Lett. 1 (3) (1998) 125.
[30] Guoyan Hou, unpublished results.
[31] A. Bo, S. Sanicharane, B. Sompalli, Q. Fan, B. Gurau, R. Liu, E.S. Smotkin, J. Phys. Chem. B 104 (31) (2000) 7377–7381.
[32] S. Sanicharane, A. Bo, B. Sompalli, B. Gurau, E.S. Smotkin, J. Electrochem. Soc. 149 (5) (2002) A554–A557.
[33] S.R. Narayanan, H. Frank, B. Jeffries-Nakamura, M. Smart, W. Chun, G. Halpert, Electrochem. Soc. Proc. 95 (23) (1995) 278–283.
[34] X. Ren, T.A. Zawodzinski, F. Uribe, H. Dai, S. Gottesfeld, Electrochem. Soc. Proc. 95 (23) (1995) 284–298.
[35] E. Gileadi, Electrode Kinetics for Chemists, Chemical Engineers, and Material Scientists, 1st ed., VCH Publishers Inc., New York, 1993, p. 5.
[36] H.N. Dinh, X. Ren, F.H. Garzon, P. Zelenay, S. Gottesfeld, J. Electroanal. Chem. 491 (2000) 222.
[37] R. Liu, H. Iddir, Q. Fan, G. Hou, A. Bo, K.L. Ley, E.S. Smotkin, Y.E. Sung, H. Kim, S. Thomas, A. Wieckowski, J. Phys. Chem. B 104 (2000) 3518–3531.
[38] A. Bo, E.S. Smotkin, manuscript in preparation.
[39] H.-W. Lei, S. Suh, B. Gurau, B. Workie, R. Liu, E.S. Smotkin, Electrochim. Acta 47 (2002) 2913–2919.